Drift kink instability in the current sheet with a kappa-distribution

Youjun Hu, Weihong Yang,[a] Yinhua Chen, Feng Huang, and Yu Zhang
CAS Key Laboratory of Basic Plasma Physics and Department of Modern Physics, University of Science and Technology of China, 230026 Hefei, China

(Received 23 May 2008; accepted 24 July 2008; published online 20 August 2008)

Superthermal particle distributions well-described by the family of κ-distributions have been observed in various astrophysical plasmas. In this paper, the drift kink instability in the current sheet with a κ-distribution is investigated in the framework of linear kinetic theory. The orbit integrals are treated numerically using the exact unperturbed particle orbits, and the resulting eigenvalue problem of the integro-differential equations is solved using the spectral method. The growth rate, eigenmode structure, and parametric dependencies of the kink mode are examined and compared with the case of the standard Harris current sheet. The results show that the drift kink instability in the κ-distribution current sheet resembles its counterpart in the standard Harris sheet, but has a smaller growth rate and real frequency for small value of κ. It is also demonstrated that a background population can enhance the growth rate of the kink mode, making the growth rate significant at the physical value of the ion-electron mass ratio. © *2008 American Institute of Physics*.
[DOI: 10.1063/1.2970099]

I. INTRODUCTION

Numerous space observations indicate that nonthermal electron and ion equilibrium structures are usually present in various astrophysical plasmas, such as, solar wind, magnetosphere, and auroral zone plasma.[1–5] The velocity distributions in these plasma structures deviate from the usual Maxwellian equilibrium distributions, having nonthermal tails in the high energy region. These features of the velocity distribution are known to be well modeled by the family of generalized Lorentzian (kappa) distributions,[6–8] a power law in particle velocity space

$$F(\boldsymbol{v}) = \frac{N}{\pi^{3/2}v_t^3}\frac{\Gamma(\kappa+1)}{\kappa^{3/2}\Gamma(\kappa-1/2)}\left(1+\frac{v_x^2+v_y^2+v_z^2}{\kappa v_t^2}\right)^{-\kappa-1}, \quad (1)$$

where $\Gamma(\kappa)$ is the Gamma function with the argument κ. The spectral index κ models the deviation of the distribution from the Maxwellian equilibrium, with the case $\kappa=\infty$ recovering the Maxwellian distribution. N denotes the particle density and v_t is the thermal velocity for a Maxwellian distribution, i.e., for $\kappa=\infty$. An effective thermal speed $\Theta=v_t\sqrt{\kappa/(\kappa-3/2)}$ can be found from the second moments of the distribution function (1), where $\Theta>v_t$ for $3/2<\kappa<\infty$ manifests the existence of a superthermal particle population.[9–12] The κ-distribution is quasi-Maxwellian at low energies and has a nonthermal tail which decreases as a power law at high energies, see Fig. 1. For typical space plasmas, the value of κ usually lies in the range of 2–6.[3]

The κ-distribution function is not only a convenient mathematical model to fit the observed velocity distributions, but also may be a particular consequence of the nonextensive entropy concepts, accounting for long range forces in astrophysical plasmas that differ from an ideal gas.[5,13] In this explanation, the spectral index κ finds the physical interpretation as the degree of nonextensivity of the system, and the κ-distribution does not need to be viewed as merely an assumption but rather as the default distribution. Every wave mode in a Maxwellian plasma then has a generalized counterpart in the plasma with a κ-distribution. The waves and instabilities in homogeneous plasma with a κ velocity distribution have been investigated in many publications.[14–17]

Recently,[18,19] the κ-distribution function was adopted in constructing the stationary solutions to the Vlasov–Maxwell system in magnetized inhomogeneous plasmas. These stationary solutions are generalizations of the standard Harris current sheet.[20] This class of generalized Harris sheets share many things with the standard Harris sheet and reduce to the standard Harris in the limit $\kappa\to\infty$. The current-sheet model based on the κ-distribution function incorporates the kinetic effects of non-Maxwellian distribution and may provide a better representation of the Earth's magnetotail where the value of κ is found to be about 5.[21] In this paper, we investigate the drift kink instabilities (DKI) in this class of current sheets.

The instabilities in current-sheet equilibria are popular topics in space physics and have received extensive investigations in the past four decades. It is believed that the triggering of magnetic reconnection in the magnetotail involves localized instabilities in the current sheet. These collisionless instabilities are crucial for determining the onset conditions and time scales of magnetic reconnection and magnetic annihilation.[22] The basic eigenmodes of the various one-dimensional equilibria are qualitatively similar, which can be roughly divided into three categories: Tearing mode,[23–28] lower-hybrid drift mode,[29–31] and drift kink mode.[32,33] The mode investigated in the present paper is a long wavelength, electromagnetic mode which clearly falls into the category of drift kink mode found in the thin Harris current sheet.[32,33] The drift kink instability was first found in the particle-in-

[a]Author to whom correspondence should be addressed. Electronic mail: whyang@ustc.edu.cn. Permanent address: Department of Modern Physics, University of Science and Technology of China, 230026 Hefei, China.

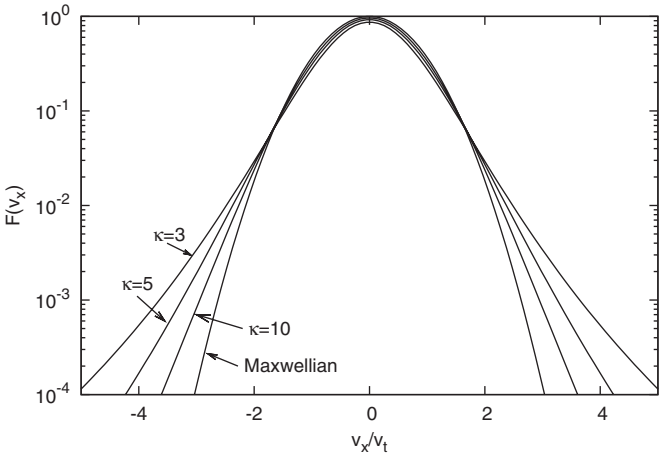

FIG. 1. Normalized κ-distribution functions for $\kappa=3$, 5, 10, and ∞.

cell simulations which assumed quite small values of the ion-electron mass ratio, $m_i/m_e \sim 25$,[34,35] and later was investigated theoretically.[32,33] DKI is a long wavelength electromagnetic mode of odd parity which propagates across the background magnetic field. It is driven by the relative streaming between particles where the phase velocity lies in the direction of the ion drift. At a realistic ion-electron mass ratio m_i/m_e, the growth rate of DKI is very small, however, in Refs. 33 and 36, it was found that the relative streaming between drifting and background ions can drive a generalized drift kink instability. The growth rate of this generalized drift kink mode is significant at the physical value of m_i/m_e. In the present paper, these properties of DKI are examined in the context of a κ-distribution current sheet using the formally exact method described in Refs. 31–33. It is found that the basic properties of DKI in the κ-distribution current sheet resemble its counterpart in the standard Harris current sheet, but has a smaller maximum growth rate for small value of κ. It is also demonstrated that a background population can enhance the growth rate of the kink mode, making the growth rate significant at the physical value of the ion-electron mass ratio.

This paper is organized as follows: The current-sheet equilibrium with a κ-distribution[18,19] is given in Sec. II. The basic equations and methods for the nonlocal instability analysis are discussed in Sec. III. The properties of DKI in the κ-distribution current sheet are examined in Sec. IV. Conclusions are given in Sec. V.

II. CURRENT-SHEET EQUILIBRIUM WITH A κ-DISTRIBUTION

With the equilibrium field given by $\boldsymbol{E}_0=0$, $\boldsymbol{B}_0=B_0(x)\boldsymbol{e}_z$, we have the following constants of the motion:

$$H_\alpha = \frac{m_\alpha(v_x^2+v_y^2+v_z^2)}{2}, \tag{2}$$

$$P_\alpha = m_\alpha v_y + \frac{q_\alpha}{c}A_0(x), \tag{3}$$

where $A_0(x)\equiv\int B_0(x)dx$ is the magnetic vector potential, m_α and q_α are particle mass and charge, respectively. α is the species label ($\alpha=i$ for the ions and $\alpha=e$ for the electrons). Using the above two constants of motion, the following distribution function can be constructed:

$$f_{0\alpha}(x,\boldsymbol{v}) = \frac{N_0}{\pi^{3/2}(2T_\alpha/m_\alpha)^{3/2}}\frac{\Gamma(\kappa+1)}{\kappa^{3/2}\Gamma(\kappa-1/2)} \times\left(1+\frac{H_\alpha - U_\alpha P_\alpha + m_\alpha U_\alpha^2/2}{\kappa T_\alpha}\right)^{-\kappa-1}, \tag{4}$$

which is a solution to the Vlasov equation. Here N_0, T_α, and U_α are multiplicative constants which are related to the number density, effective temperature, and drift velocity in the y direction, respectively. From Eq. (4) it is straightforward to calculate the following velocity moments of the distribution function,

$$n_\alpha(x) \equiv \int_{-\infty}^{\infty} f_{0\alpha}(x,\boldsymbol{v})d\boldsymbol{v} = N_0\left[1-\frac{q_\alpha U_\alpha A_0(x)}{\kappa T_\alpha c}\right]^{-\kappa+1/2}, \tag{5}$$

$$\langle v_y\rangle_\alpha \equiv \frac{1}{n_\alpha}\int_{-\infty}^{\infty} v_y f_{0\alpha}(x,\boldsymbol{v})d\boldsymbol{v} = U_\alpha. \tag{6}$$

To enforce charge neutrality, Eq. (5) requires

$$\frac{U_i}{T_i} = -\frac{U_e}{T_e} \tag{7}$$

and all the Maxwell's equations are satisfied except for the y component of the Ampere's law, which requires

$$-\frac{d^2A_0(x)}{dx^2} = \frac{4\pi e}{c}(n_i\langle v_y\rangle_i - n_e\langle v_y\rangle_e). \tag{8}$$

After substituting Eqs. (5) and (6) into this equation, it takes the form

$$\frac{d^2\bar{A}_0}{d\bar{x}^2} = \left(1+\frac{2\bar{A}_0}{\kappa}\right)^{-\kappa+1/2}, \tag{9}$$

where the dimensionless quantities are given by

$$\bar{x} = \frac{x}{L}, \quad \bar{A}_0 = -\frac{U_i e A_0}{2cT_i}.$$

Here $L=-2cT_i/(b_0eU_i)$ and $b_0\equiv\sqrt{8\pi N_0(T_i+T_e)}$.

When $\kappa\to\infty$, we have $\lim_{\kappa\to\infty}(1+2\bar{A}_0/\kappa)^{-\kappa+1/2} = \exp(-2\bar{A}_0)$ and Eq. (9) takes the form

$$\frac{d^2\bar{A}_0}{d\bar{x}^2} = \exp(-2\bar{A}_0) \tag{10}$$

with its solution being the well-known Harris current-sheet solution $\bar{A}_0(\bar{x})=\ln(\cosh\bar{x})$, and the corresponding magnetic field $\bar{B}(\bar{x})=\tanh(\bar{x})$.

When κ is finite, the solution to Eq. (9) can be expressed in a formal analytic form.[18] From the practical view, however, it is straightforward to solve Eq. (9) by a direct numerical method. With the boundary condition

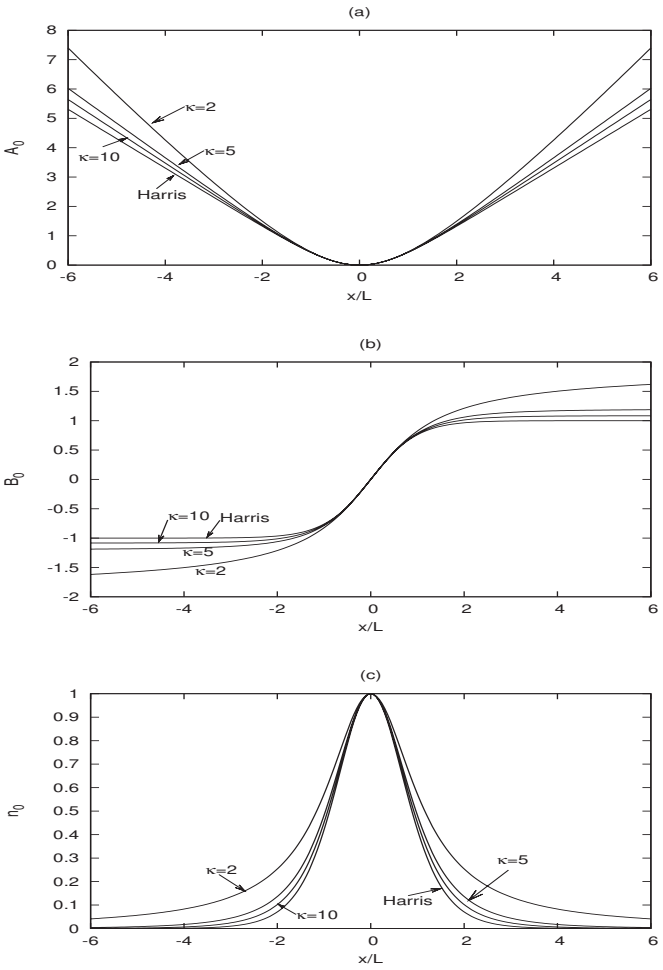

FIG. 2. Normalized vector potential, magnetic field, and number density of the κ-distribution current sheet for $\kappa=2,5,10,\infty$. The case of $\kappa=\infty$ corresponds to the Harris sheet.

$$\bar{A}_0(0)=0, \quad \frac{d\bar{A}_0(0)}{d\bar{x}}=0$$

the solutions are shown in Fig. 2(a) for $\kappa=2$, 5, 10, and ∞. The corresponding magnetic field and number density are shown in Figs. 2(b) and 2(c).

In the above, we briefly give the derivation of the κ-distribution current sheet, which replaces the Gaussian function $\exp(-x^2)$ in the distribution function of the standard Harris current sheet by the κ-distribution $(1+x^2/\kappa)^{-\kappa-1}$. It was pointed out in Ref. 19 that the effective temperature of this κ-distribution current sheet is divergent in the asymptotic region and a uniform background population can address this situation, making the effective temperature finite in the asymptotic region. In the present paper, a uniform background population of the form

$$f_{b\alpha}(\boldsymbol{v})=\frac{n_b}{\pi^{3/2}v_{t\alpha}^3}\frac{\Gamma(\kappa+1)}{\kappa^{3/2}\Gamma(\kappa-1/2)}\left(1+\frac{v_x^2+v_y^2+v_z^2}{\kappa v_{t\alpha}^2}\right)^{-\kappa-1} \tag{11}$$

is included in the current sheet. The effects of this background population on the drift kink mode are investigated in Sec. IV E.

III. BASIC EQUATIONS AND METHODS FOR THE NONLOCAL STABILITY ANALYSIS

In this section, we provide the basic theory for the nonlocal kinetic stability analysis of the κ-distribution current-sheet equilibrium described in Sec. II. The methods for dealing with the orbit integral and solving the resulting eigenvalue problem of the integro-differential equations are from Refs. 31–33, where these methods are applied to the Harris current-sheet equilibrium.

A. Perturbed distribution function and its velocity moments

The linearized Vlasov equation is given by

$$\frac{\partial f_{1\alpha}}{\partial t}+\boldsymbol{v}\cdot\nabla f+\frac{\boldsymbol{v}\times\boldsymbol{B}_0}{c}\cdot\nabla_v f_{1\alpha}$$
$$=-\frac{q_\alpha}{m_\alpha}\left(\boldsymbol{E}_1+\frac{\boldsymbol{v}\times\boldsymbol{B}_1}{c}\right)\cdot\nabla_v f_{0\alpha}, \tag{12}$$

where $\boldsymbol{B}_0$ is the equilibrium magnetic field, $f_{0\alpha}$ is the equilibrium distribution function given by Eq. (4), and $f_{1\alpha}$, $\boldsymbol{E}_1$, $\boldsymbol{B}_1$ are the perturbed distribution function, electric field, and magnetic field, respectively. The perturbed electromagnetic fields are described by the scalar potential ϕ_1 and vector potential $\boldsymbol{A}_1$,

$$\boldsymbol{E}_1=-\nabla\phi_1-\frac{1}{c}\frac{\partial\boldsymbol{A}_1}{\partial t}, \quad \boldsymbol{B}_1=\nabla\times\boldsymbol{A}_1$$

and we consider perturbations of the form

$$\phi_1=\hat{\phi}(x)\exp[i(k_y y-\omega t)],$$

$$\boldsymbol{A}_1=\hat{\boldsymbol{A}}(x)\exp[i(k_y y-\omega t)].$$

Integrating along the unperturbed particle orbits, we get the perturbed distribution function $f_{1\alpha}$,

$$f_{1\alpha}(x,\boldsymbol{v})=-\frac{q_\alpha G_{0\alpha}}{T_a}\left\{\hat{\phi}(x)-\frac{U_\alpha}{c}\hat{A}_y(x)+i(\omega-k_y U_\alpha)\right.$$
$$\times\int_{-\infty}^{0}\left[\hat{\phi}(x')-\frac{\boldsymbol{v}\cdot\hat{\boldsymbol{A}}(x')}{c}\right]$$
$$\left.\times\exp[ik_y(y'-y)-i\omega\tau]\right\}, \tag{13}$$

where $x'(\tau)$, $y'(\tau)$, $\boldsymbol{v}'(\tau)$ are particle orbits in the equilibrium field. The initial condition at $\tau=0$ is $x'=x$, $y'=y$, $\boldsymbol{v}'=\boldsymbol{v}$ and $G_{0\alpha}$ is given by

$$G_{\alpha 0}=\frac{N_0}{\pi^{3/2}v_{t\alpha}^3}\frac{\Gamma(\kappa+1)}{\kappa^{3/2}\Gamma(\kappa-1/2)}\frac{\kappa+1}{\kappa}$$
$$\times\left[1-\frac{U_\alpha q_\alpha A_0}{\kappa T_\alpha c}+\frac{v_x^2+v_z^2+(v_y-U_a)^2}{\kappa v_{t\alpha}^2}\right]^{-\kappa-2},$$

where $v_{t\alpha}\equiv\sqrt{2T_\alpha/m_\alpha}$.

From the perturbed distribution function Eq. (13), it is straightforward to calculate the perturbed charge density

$$\rho_\alpha(x) \equiv q_\alpha \int_{-\infty}^{\infty} dv_x \int_{-\infty}^{\infty} dv_y \int_{-\infty}^{\infty} dv_z f_{1\alpha}(x,\boldsymbol{v})$$
$$= -\frac{q_\alpha^2 N_0}{T_\alpha}\left\{\left[\hat{\phi}(x) - \frac{U_\alpha}{c}\hat{A}_y(x)\right]\frac{\kappa - 1/2}{\kappa} \times\left[1 - \frac{U_\alpha q_\alpha A_0(x)}{\kappa T_\alpha c}\right]^{-\kappa-1/2} - (\omega - k_y U_\alpha) \times\frac{i}{\pi v_{t\alpha}^2}\frac{\kappa^2 - 1/4}{\kappa^2}\int_{-\infty}^{\infty} dv_x \int_{-\infty}^{\infty} dv_y \left[1 - \frac{U_\alpha q_\alpha A_0(x)}{\kappa T_\alpha c} + \frac{v_x^2 + (v_y - U_\alpha)^2}{\kappa v_{t\alpha}^2}\right]^{-\kappa-3/2} S_\alpha\right\} \tag{14}$$

and the perturbed current density in the x direction

$$J_{\alpha x}(x) \equiv q_a \int_{-\infty}^{\infty} v_x dv_x \int_{-\infty}^{\infty} dv_y \int_{-\infty}^{\infty} dv_z f_{1\alpha}(x,\boldsymbol{v})$$
$$= -\frac{q_\alpha^2 N_0}{T_\alpha} i(\omega - k_y U_\alpha)\frac{1}{\pi v_{t\alpha}^2}\frac{\kappa^2 - 1/4}{\kappa^2} \times\int_{-\infty}^{\infty} v_x dv_x \int_{-\infty}^{\infty} dv_y \left[1 - \frac{U_\alpha q_\alpha A_0(x)}{\kappa T_\alpha c} + \frac{v_x^2 + (v_y - U_\alpha)^2}{\kappa v_{t\alpha}^2}\right]^{-k-3/2} S_\alpha, \tag{15}$$

where S_α is given by

$$S_\alpha = \int_{-\infty}^{0} d\tau \left[\hat{\phi}(x') - \frac{v_x' \hat{A}_x(x') + v_y' \hat{A}_y(x')}{c}\right] \times\exp[ik_y(y' - y) - i\omega\tau]. \tag{16}$$

In the equilibrium field $B_0 = B(x)\boldsymbol{e}_z$, the particle motion in the z direction is given by

$$z' = z + v_z \tau, \quad v_z' = v_z$$

while x', y', v_x' and v_y' are independent of v_z, thus the integral over the v_z component of velocity space can be performed. In the above, the integral over v_z has been evaluated analytically.

B. Methods for treating the orbit integral

The orbit integral in Eq. (16) is an improper integral with infinite integral limit. As pointed out by Daughton,[32,33] using the periodic property of the particle motion, the integral can be calculated by following particles for a single period. As for the case of the κ-distribution sheet, although the equilibrium magnetic field are different from the standard Harris magnetic field, the periodic property of the particle motion remains the same. To calculate the period of a particle, we first calculate its location in the x direction where its v_x is zero, then integrate between these two locations (turning points) to calculate the time the particle spends in travelling between the two turning points. From the constants of the motion, we have

$$v_x^2(x) = \frac{2H_{\perp\alpha}}{m_a} - \frac{\left[P_\alpha - \frac{q_\alpha}{c}A_0(x)\right]^2}{m_\alpha^2}, \tag{17}$$

where $H_{\perp\alpha} \equiv m_\alpha(v_x^2 + v_y^2)/2$. The zero points of Eq. (17) are possible turning points. The time for the particle to travel between the tuning points is given by

$$t_{p\alpha} = 2\int_{x_1}^{x_2} \frac{dx}{v_x(x)},$$

which is the period for the particle's $v_x'(\tau)$, $v_y'(\tau)$, $x'(\tau)$. Here x_1, x_2 are two turning points for this particle. Although $y'(\tau)$ is not a periodic function, it has the property

$$y'(\tau + nt_{p\alpha}) = y'(\tau) + n\Delta,$$

where $\Delta \equiv \int_0^{t_{p\alpha}} v_y'(\tau)d\tau$ and n is an integer. Using these properties of the unperturbed orbits, the integral in Eq. (16) can be expressed as

$$S_\alpha = \frac{1}{1 - \exp[i(\omega t_{p\alpha} - k_y \Delta_\alpha)]} I_0,$$

where

$$I_0 = \int_{-t_{p\alpha}}^{0} d\tau \left[\hat{\phi}(x') - \frac{v_x' \hat{A}_x(x') + v_y' \hat{A}_y(x')}{c}\right] \times\exp[ik_y(y' - y) - i\omega\tau]$$

and this form has the advantage that the orbit of a particle needs to be followed for only a single period.

C. Maxwell's equations

We work in the Coulomb gauge

$$\nabla \cdot \boldsymbol{A}_1 = 0. \tag{18}$$

Maxwell's equations take the form

$$-\nabla^2 \phi_1 = 4\pi(\rho_i + \rho_e), \tag{19}$$

$$-\nabla^2 A_{1x} = \frac{4\pi}{c}(J_{ix} + J_{ex}) - \frac{1}{c}\frac{\partial^2 \phi_1}{\partial t \partial x} - \frac{1}{c^2}\frac{\partial^2 A_{1x}}{\partial t^2}, \tag{20}$$

$$-\nabla^2 A_{1y} = \frac{4\pi}{c}(J_{iy} + J_{ey}) - \frac{1}{c}\frac{\partial^2 \phi_1}{\partial t \partial y} - \frac{1}{c^2}\frac{\partial^2 A_{1y}}{\partial t^2}, \tag{21}$$

$$-\nabla^2 A_{1z} = \frac{4\pi}{c}(J_{iz} + J_{ez}) - \frac{1}{c}\frac{\partial^2 \phi_1}{\partial t \partial z} - \frac{1}{c^2}\frac{\partial^2 A_{1z}}{\partial t^2}. \tag{22}$$

When the field perturbation is of the form $h(x)\exp[i(k_y y - \omega t)]$, it can be proved that Eq. (21) is redundant in the Maxwell–Vlasov system, and thus should be removed from the system. In the resulting system, A_{1z} become independent of all the others, namely, A_{1x}, A_{1y}, and ϕ_1. This indicates two independent polarizations exist. In this analysis we focus on the latter polarization, i.e., A_{1x}, A_{1y}, and ϕ_1. For this polarization, Eqs. (14), (15), (19), and (20) along with the Coulomb gauge (18) constitute a complete system.

D. Spectral method for the eigenvalue problem

In the spectral method,[33,37] the unknown functions $\hat{\phi}(x)$, $\hat{A}_x(x)$, $\hat{A}_y(x)$ are assumed to be able to be approximated by the linear combination of a series of basis functions,

$$\hat{\phi}(x) = \sum_{n=0}^{N-1} C_n \Psi_n(x), \quad \hat{A}_x(x) = \sum_{n=0}^{N-1} C_{N+n} \Psi_n(x),$$

$$\hat{A}_y(x) = \sum_{n=0}^{N-1} C_{2N+n} \Psi_n(x),$$

with the coefficients C_i unknown. Using these expression in the complete system discussed in Sec. III C results in the following matrix equation:

$$M_{ij} C_j = 0, \tag{23}$$

where the elements of the $3N \times 3N$ matrix M_{ij} are computed from the inner product between the N basis functions and Eqs. (18)–(20). The inner product between $\Psi_n(x)$ and a function $g(x)$ is defined by

$$\langle \Psi_n | g \rangle \equiv \int_{-\infty}^{\infty} \Psi_n(x) g(x) dx.$$

Nontrivial solutions to Eq. (23) exist for values of the complex frequency ω such that

$$\det(M) = 0$$

which is the dispersion relation and the nontrivial solutions give the expansion coefficients for the eigenfunctions.

The basis functions used in the present paper are Hermite functions[33,37]

$$\Psi_n(x) = \frac{1}{\pi^{1/4}\sqrt{2^n n!}} \exp\left(-\frac{x^2}{2}\right) H_n(x),$$

where $H_n(x)$ is the Hermite polynomial of order n. The Hermite functions satisfy the necessary boundary condition that the field perturbation vanishes at infinity.

IV. RESULTS

In this section, using the method described in Sec. III, we calculate the growth rate and mode structure of the drift kink mode in the κ-distribution current sheet. In the process of computing the unperturbed orbits, we use the particle's cyclotron frequency in the asymptotic Harris magnetic field $\Omega_{\alpha 0} \equiv b_0 e / m_\alpha c$ to normalize time. The space is normalized by L. The normalized perturbed field is given by

$$\bar{\phi} = \frac{\hat{\phi}}{\phi_0}, \quad \bar{A}_x = \frac{\hat{A}_x}{\phi_0 c / v_{ti}}, \quad \bar{A}_y = \frac{\hat{A}_y}{\phi_0 c / v_{ti}},$$

where $\phi_0 \equiv 4\pi e^2 N_0 L^2$. We use Newton's method to calculate the root of $\det(M)=0$, and use singular value decomposition (SVD) to calculate the corresponding nontrivial solutions. In addition, for the low frequency, long wavelength mode considered in the present paper, the displacement current and the $\nabla^2 \varphi$ terms in Poisson's equation can be safely neglected. In Secs. IV A–IV D, we consider a κ-distribution current sheet without a background population, while in Sec. IV E, we consider the effect of the background population.

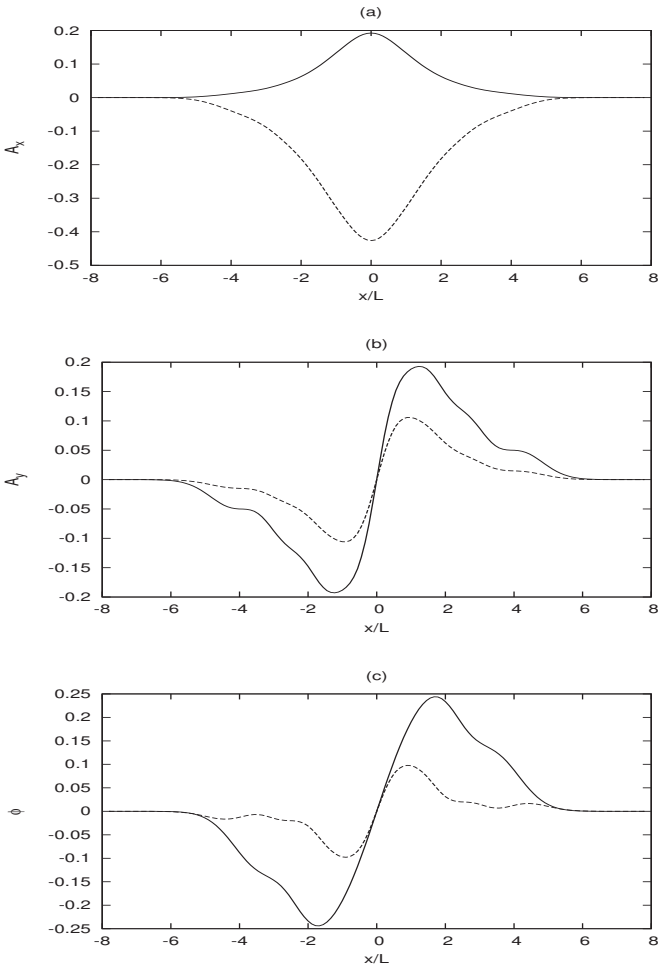

FIG. 3. Typical eigenfunction for the kink mode for the parameters $\kappa=3$, $m_i/m_e=16$, $\rho_i/L=0.7$, $T_i/T_e=1$, and $k_y L=0.8$. The solid line represents the real part of each quantity, while the dashed line is the imaginary part.

A. Typical eigenfunction

A typical eigenfunction for the drift kink mode is shown in Fig. 3 for the parameters $\kappa=3$, $m_i/m_e=16$, $\rho_i/L=0.7$, $T_i/T_e=1$, and $k_y L=0.8$. Here $\rho_i \equiv v_{ti}/\Omega_{i0}$ is the ion gyroradius defined with a gyrofrequency calculated from the magnetic field b_0. For this example, the Hermite expansion was truncated at $N=14$ terms and the resulting growth rate and real frequency are $\mathrm{Im}(\omega)/\Omega_{i0}=0.11$ and $\mathrm{Re}(\omega)/\Omega_{i0}=0.36$, with phase velocity in the direction of the ion drift. For the standard Harris sheet ($\kappa=\infty$) with the same parameter as above, the growth rate and real frequency are $\mathrm{Im}(\omega)=0.16$ and $\mathrm{Re}(\omega)/\Omega_{i0}=0.36$.[33] The eigenfunctions shown in Fig. 3 are odd parity in $\hat{A}_y(x)$, $\hat{\phi}(x)$ and even parity in $\hat{A}_x(x)$. These parity properties are consistent with the results of the standard Harris sheet.

B. Dependence on κ

In Fig. 4, the growth rate and real frequency of the kink mode are given as a function of $k_y L$ for the parameters $\kappa=5$, 10, and ∞. The other parameters are $\rho_i/L=1$, $T_i/T_e=1$,

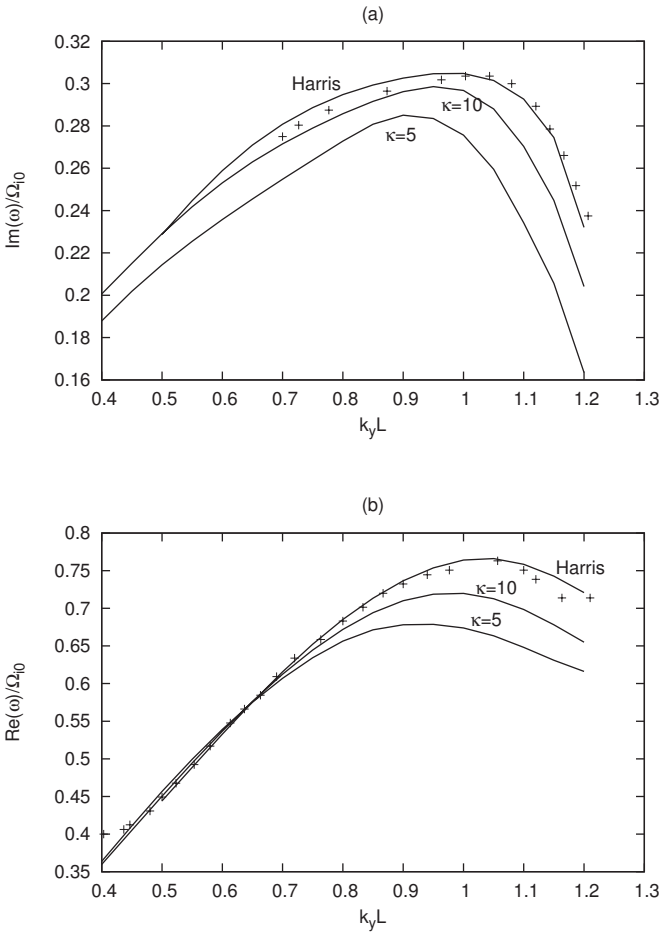

FIG. 4. Growth rate and real frequency of the kink mode as a function of k_yL for $\kappa=5$, 10, and ∞. The other parameters are $m_i/m_e=16$, $\rho_i/L=1$, $T_i/T_e=1$. The cross symbols shown in the figure are results of Ref. 33 for the Harris sheet.

and $m_i/m_e=16$. The case $\kappa=\infty$ corresponds to the Harris current sheet. Also shown in Fig. 4 are results in Ref. 33 for the Harris sheet. DKI is a long wavelength instability with typical wavelength $k_yL\sim 1$. In Fig. 4, the wavelength of maximum growth for the DKI is about at $k_yL=1$. The maximum growth rate increases as the value of κ increases.

In Fig. 5, the maximum growth rate and the corresponding real frequency are given as a function of κ for the parameters $\rho_i/L=1$, $T_i=T_e$, and $m_i/m_e=16$. Growth rates are maximized over wavelength $k_yL\sim 1$. The maximum growth rate increases with the increasing κ and approaches an asymptotic value at large values of κ. The corresponding real frequency also increases as κ increases.

C. Dependence on the sheet thickness and ion-electron temperature ratio

In Fig. 6, the maximum growth rate are given as a function of ρ_i/L for the parameters $\kappa=4$, 5, and ∞. In Fig. 7, the maximum growth rate are given as a function of T_i/T_e for the parameters $\kappa=4$ and ∞. The $\kappa=\infty$ (Harris) case shown in Figs. 6 and 7 are the results of Ref. 33.

The driving factor for the kink mode is the relative drift velocity between the ions and electrons, U_i-U_e, which can be expressed in dimensionless form as

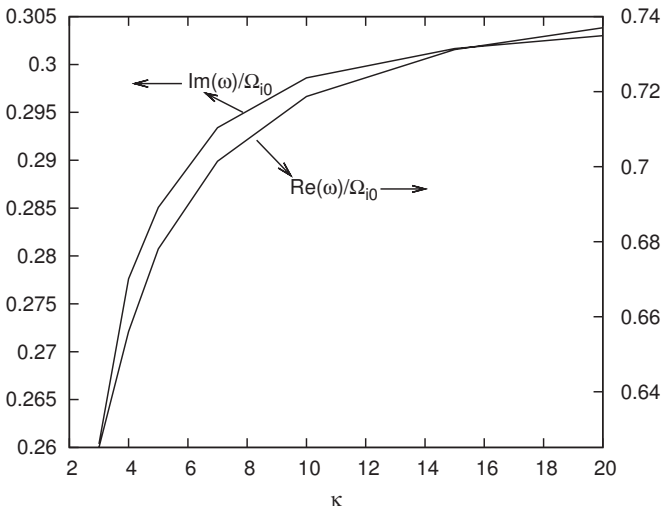

FIG. 5. Maximum growth rate and the corresponding real frequency as a function of κ for the parameters $m_i/m_e=16$, $\rho_i/L=1$, and $T_i/T_e=1$. Growth rates are maximized over wavelength $k_yL\sim 1$.

$$\frac{|U_i-U_e|}{v_{ti}}=\frac{\rho_i}{L}\left(1+\frac{T_e}{T_i}\right).$$

Therefore, it is expected that the growth rate should increase with ρ_i/L and T_e/T_i. These trends are confirmed in Fig. 6 for the sheet thickness and in Fig. 7 for the temperature ratio. These results are consistent with the results of the Harris current sheet.[33]

D. Dependence on ion-electron mass ratio

In Fig. 8, the growth rate and real frequency of the kink mode are given as a function of k_yL for the parameters $m_i/m_e=8$, 16, and 32. The other parameters are $\kappa=5$, $\rho_i/L=1$ $T_i=T_e$. For equal masses $m_i=m_e$ and temperatures $T_i=T_e$, the kink mode is a purely growing instability. As the mass ratio increases, the mode develops a real frequency with phase velocity in the direction of the ion diamagnetic drift. The wavelength of maximum growth for DKI is in the range $k_yL\sim 1$ and shifts towards shorter wavelength as the

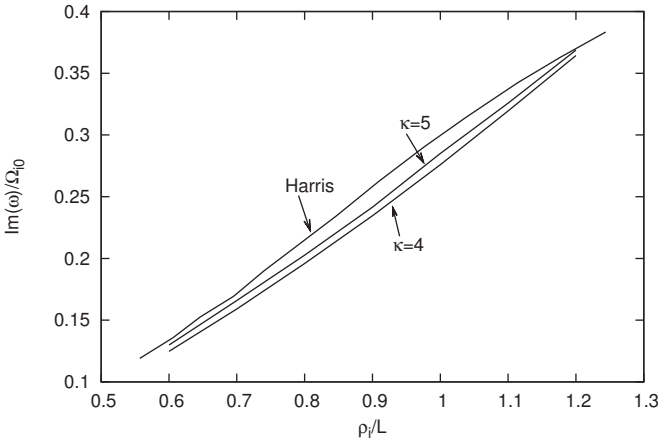

FIG. 6. Maximum growth rate of the kink mode as a function of ρ_i/L for $\kappa=4$, 5, and ∞. The other parameters are $T_i/T_e=1$, $m_i/m_e=16$. The Harris case shown in the figure are the results in Ref. 33.

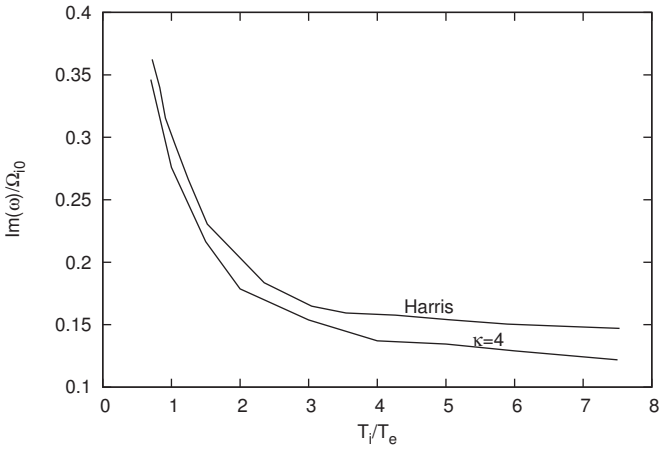

FIG. 7. Maximum growth rate of the kink mode as a function of T_i/T_e for $\kappa=4$ and ∞. The other parameters are $\rho_i/L=1$, $m_i/m_e=16$. The Harris case shown in the figure are the results of Ref. 33.

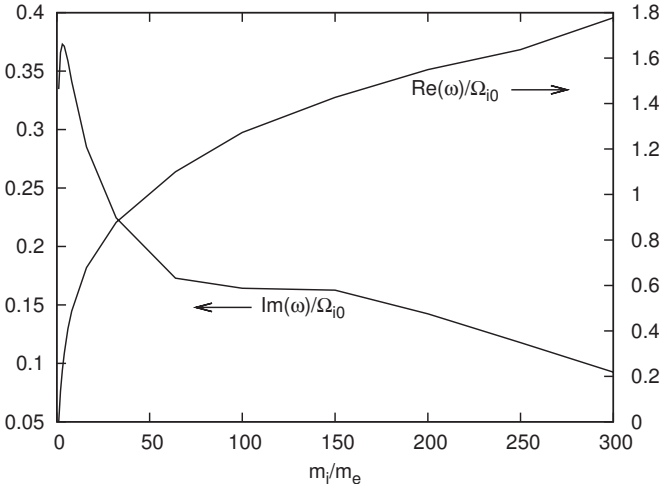

FIG. 9. Maximum growth rate and the corresponding real frequency as a function of m_i/m_e for the parameters $\kappa=5$, $\rho_i/L=1$, and $T_i/T_e=1$.

mass ratio increases. At larger value of ion-electron mass ratio $m_i/m_e=32$, the real frequency of DKI is well approximated by the ion diamagnetic frequency k_yU_i in the long wavelength region. These properties of DKI are consistent with its counterpart in the Harris current sheet.[32,33]

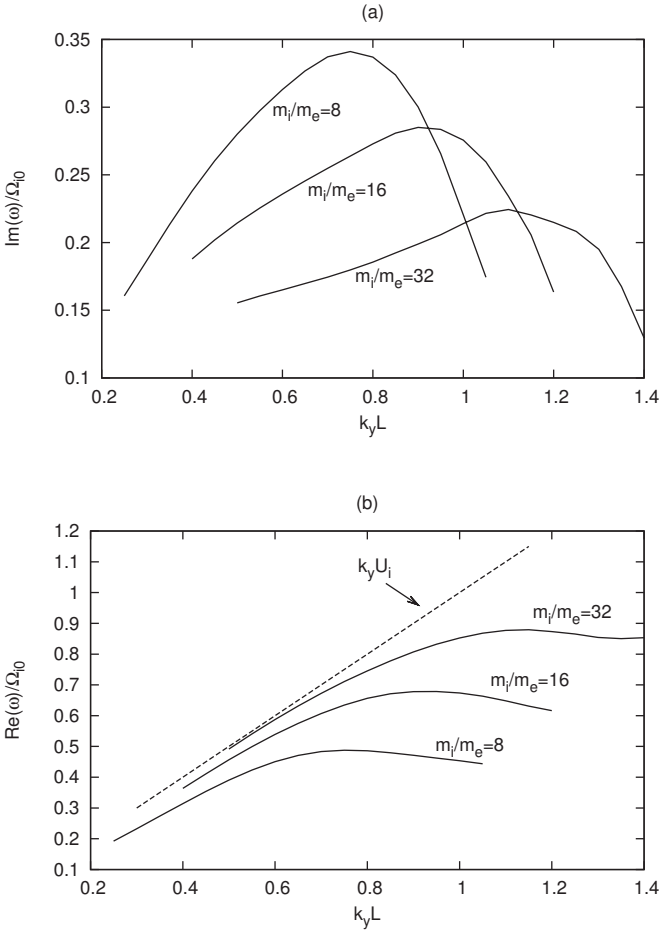

FIG. 8. Growth rate and real frequency of the kink mode as a function of k_yL for $m_i/m_e=8$, 16, and 32. The other parameters are $\kappa=5$, $\rho_i/L=1$, $T_i/T_e=1$. The dashed line in (b) corresponds to the ion diamagnetic frequency $\omega_{*i}=k_yU_i$.

It is known that DKI in the Harris current sheet has significant growth rates only at low ion-electron mass ratios.[33] At the realistic mass ratio, the growth rate decreases to a very small value. These results remain the same for the κ-distribution current sheet. In Fig. 9, the maximum growth rate of DKI are given as a function of m_i/m_e for the parameters $\kappa=5$, $\rho_i/L=1$, and $T_i/T_e=1$. In the region of very low mass ratio, the growth rate increases with the increasing mass ratio, while in the region of larger ratio, the growth rate decreases as the mass ratio increases. The corresponding real frequency increases with the increasing mass ratio and the wavelength for the maximum growth rate shifts towards shorter wavelength as the mass ratio increases.

E. Effect of background population

As pointed out in Refs. 32 and 33, a uniform background population introduces new relative drift between particles, which can excite a generalized kink mode in the Harris current sheet. With a uniform background population included in the current sheet, the kink mode has significant growth rate at the physical value of the ion-electron mass ratio. For a κ-distribution current sheet, the background population takes the form of Eq. (11). This κ-distribution background population has the same effect as the Gaussian distribution background population in the Harris sheet. In Fig. 10 the growth rates are given as a function of background density for the realistic value of mass ratio $m_i/m_e=1836$. The other parameters are $\kappa=5$, $T_i/T_e=1$, $\rho_i/L=1$, $k_yL=0.8$. The parameters for the background plasma (κ, m_i/m_e, T_i/T_e) are identical to the drifting distributions. As shown in Fig. 10, the growth rates of DKI in this case are significant and increase as the background density increases.

As mentioned above, a background population makes the temperature finite in the asymptotic region, which shows that the presence of a background population can be important from the standpoint of mathematically modeling the current sheet with a κ-distribution. On the other hand, there has been some observational evidence which indicates that a background population may exist in a real current sheet.[36]

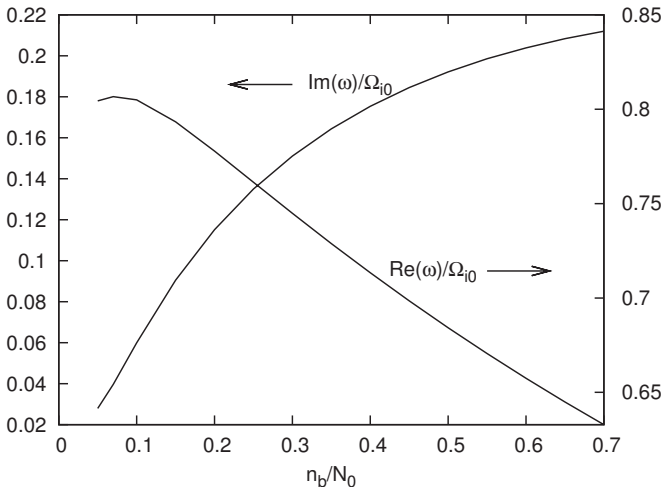

FIG. 10. Growth rate and the corresponding real frequency as a function of background density for the parameters $\kappa=5$, $m_i/m_e=1836$, $\rho_i/L=1$, $T_i/T_e=1$, and $k_yL=0.8$.

For example, in the magnetotail the presence of the ion background population can be due to the lobe plasma or due to ionospheric ions. These observations make the generalized drift kink mode relevant to the stability of the magnetotail. The cluster observations[38] also indicate that the current-sheet flapping motion in the magnetotail may be a result of the kink mode.

V. CONCLUSIONS

In this paper, the properties of the drift kink mode in the current sheet with a κ-distribution are examined using the formally exact method described in Refs. 31–33. The growth rates, eigenmode structure, and parametric dependencies of the kink mode are presented and compared with the standard Harris current sheet. The results indicate that the drift kink mode in the κ-distribution current sheet resembles its counterpart in the standard Harris sheet, but has smaller growth rate and real frequency. The maximum growth rate of the kink mode in the κ-distribution current sheet decreases with the decreasing value of κ. It was also demonstrated that a background population can enhance the growth rate of the kink mode, making the growth rate significant at the physical value of the ion-electron mass ratio.

The current-sheet model based on the κ-distribution function incorporates the kinetic effects of non-Maxwellian distribution and provides a new starting point for the investigation of plasma stability in inhomogeneous plasmas. In addition to the kink mode considered in this paper, lower-hybrid and tearing mode in the κ-distribution current sheet can be analyzed by the same method and these remain for the future work.

ACKNOWLEDGMENTS

This work was supported by the National Science Foundation of China under Grant Nos. 10775134 and 40336052.

[1] V. Formisano, G. Moreno, and F. Palmiotto, J. Geophys. Res. **78**, 3714, DOI: 10.1029/JA078i019p03714 (1973).
[2] D. A. Mendis and M. Rosenberg, Annu. Rev. Astron. Astrophys. **32**, 419 (1994).
[3] J. D. Scudder, E. C. Sittler, and H. S. Bridge, J. Geophys. Res. **86**, 8157, DOI: 10.1029/JA086iA10p08157 (1981).
[4] E. Marsch, K.-H. Mühlhäuser, R. Schwenn, H. Rosenbauer, W. Pillip, and F. M. Neubauer, J. Geophys. Res. **87**, 52, DOI: 10.1029/JA087iA01p00052 (1982).
[5] M. P. Leubner, Phys. Plasmas **11**, 1308 (2004).
[6] A. Papoulis, *Probability, Random Variables, and Stochastic Processes*, 2nd ed (McGraw-Hill, New York, 1984), p. 104.
[7] M. Collier, Geophys. Res. Lett. **20**, 1531, DOI: 10.1029/93GL01702 (1993).
[8] V. M. Vasyliunas, J. Geophys. Res. **73**, 2839, 10.1029/JA073i009p02839 (1968).
[9] M. Collier, J. Geophys. Res. **104**, 28559, DOI: 10.1029/1999JA900355 (1999).
[10] M. Collier, A. Roberts, and A. Vinas, Adv. Space Res. **41**, 1704 (2008).
[11] M. Collier and D. C. Hamilton, Geophys. Res. Lett. **22**, 303, DOI: 10.1029/94GL02997 (1995).
[12] M. Collier, Geophys. Res. Lett. **22**, 2673, DOI: 10.1029/95GL02350 (1995).
[13] M. P. Leubner, Astrophys. Space Sci. **282**, 573 (2002).
[14] R. L. Mace, Phys. Plasmas **10**, 2181 (2003).
[15] R. L. Mace, Phys. Plasmas **11**, 507 (2004).
[16] T. Cattaert, M. A. Hellberg, and R. L. Mace, Phys. Plasmas **14**, 082111 (2007).
[17] M. N. S. Qureshi, H. A. Shah, G. Murtaza, S. J. Schwartz, and F. Mahmood, Phys. Plasmas **11**, 3819 (2004).
[18] W. Z. Fu and L. N. Hau, Phys. Plasmas **12**, 070701 (2005).
[19] P. H. Yoon, A. T. Lui, and R. B. Sheldon, Phys. Plasmas **13**, 102108 (2006).
[20] E. G. Harris, Nuovo Cimento **23**, 115 (1962).
[21] S. P. Christon, D. J. Williams, D. G. Mitchell, L. A. Frank, and C. Y. Huang, J. Geophys. Res. **94**, 13409, DOI: 10.1029/JA094iA10p13409 (1989).
[22] M. I. Sitnov, A. T. Y. Lui, P. N. Guzdar, and P. H. Yoon, J. Geophys. Res. **109**, A03205, DOI: 10.1029/2003JA010123 (2003).
[23] B. Coppi, G. Laval, and R. Pellat, Phys. Rev. Lett. **16**, 1207 (1966).
[24] J. Chen and Y. C. Lee, Phys. Fluids **28**, 2137 (1985).
[25] G. R. Burkhart and J. Chen, Phys. Fluids B **1**, 1578 (1989).
[26] T. Matsui and W. Daughton, Phys. Plasmas **15**, 012901 (2008).
[27] W. Daughton and H. Karimabadi, J. Geophys. Res. **110**, A03217, DOI: 10.1029/2004JA010751 (2005).
[28] J. Chen and P. Palmadesso, Phys. Fluids **27**, 1198 (1984).
[29] R. C. Davidson, N. T. Gladd, C. S. Wu, and J. D. Huba, Phys. Fluids **20**, 301 (1977).
[30] J. D. Huba, J. F. Drake, and N. T. Gladd, Phys. Fluids **23**, 552 (1980).
[31] W. Daughton, Phys. Plasmas **10**, 3103 (2003).
[32] W. Daughton, J. Geophys. Res. **103**, 29429, DOI: 10.1029/1998JA900028 (1998).
[33] W. Daughton, Phys. Plasmas **6**, 1329 (1999).
[34] Z. Zhu and R. M. Winglee, J. Geophys. Res. **101**, 4885, DOI: 10.1029/95JA03144 (1996).
[35] P. L. Pritchett, F. V. Coroniti, and V. K. Decyk, J. Geophys. Res. **101**, 27413, DOI: 10.1029/96JA02665 (1996).
[36] H. Karimabadi, W. Daughton, P. L. Pritchett, and D. Krausss-Varban, J. Geophys. Res. **108**, 1400, DOI: 10.1029/2003JA010026 (2003).
[37] J. P. Boyd, *Chebyshev and Fourier Spectral Methods* (Dover, New York, 2000), p. 346.
[38] V. Sergeev, A. Runov, W. Baumjohann, R. Nakamura, T. L. Zhang, and M. Volwerk, Geophys. Res. Lett. **30**, 1327, DOI: 10.1029/2002GL016500 (2003).